Fungal transformation of mineral substrata of biodeteriorated medieval murals in Saint Sophia's cathedral, Kyiv, Ukraine

Fomina, Marina; Cuadros, Javier; Pinzari, Flavia; Hryshchenko, Nataliya; Najorka, Jens; Gavrilenko, Marina

Published in:
International Biodeterioration and Biodegradation

DOI:
10.1016/j.ibiod.2022.105486

Publication date:
2022

International Biodeterioration & Biodegradation 175 (2022) 105486

Contents lists available at ScienceDirect

International Biodeterioration & Biodegradation

journal homepage: www.elsevier.com/locate/ibiod

Fungal transformation of mineral substrata of biodeteriorated medieval murals in Saint Sophia's cathedral, Kyiv, Ukraine

Marina Fomina [a,b,*], Javier Cuadros [c], Flavia Pinzari [d,e], Nataliya Hryshchenko [f], Jens Najorka [g], Marina Gavrilenko [a], Ji Won Hong [h], Geoffrey Michael Gadd [i,j]

[a] Zabolotny Institute of Microbiology and Virology, NAS of Ukraine, Zabolotny Str. 154, Kyiv, 03143, Ukraine
[b] National Reserve "Sophia of Kyiv", Kyiv, 01001, Ukraine
[c] Department of Earth Sciences, Natural History Museum, London, SW7 5BD, UK
[d] Department of Life Sciences, Natural History Museum, London, SW7 5BD, UK
[e] Institute for Biological Systems, National Research Council, Rome, Monterotondo, 00015, Italy
[f] Institute of Molecular Biology and Genetics, NAS of Ukraine, Kyiv, 03680, Ukraine
[g] Core Research Laboratories, Natural History Museum, London, SW7 5BD, UK
[h] Kyungpook National University, Daegu, 41566, South Korea
[i] Geomicrobiology Group, School of Life Sciences, University of Dundee, Dundee, DD1 5EH, Scotland, UK
[j] State Key Laboratory of Heavy Oil Processing, Beijing Key Laboratory of Oil and Gas Pollution Control, College of Chemical Engineering and Environment, China University of Petroleum, 18 Fuxue Road, Changping District, Beijing, 102249, China

ARTICLE INFO

This article is dedicated to the courageous Ukrainian people.

Keywords:
Saint Sophia's of Kyiv
Fresco deterioration
SEM-EDS
Micro-XRD
qPCR absolute abundance estimation
Ca-malate biomineralization

ABSTRACT

Microbial activity following invasion of human-made structures and artifacts can have profound social and economic consequences including the permanent loss of cultural heritage. The unique frescoes in the 11th century Saint Sophia's Cathedral (Kyiv, Ukraine) have recently suffered from dark-spot biodeterioration. The aim of this work was to elucidate the microbial nature of biodeterioration and the biogeochemical processes occurring in the areas of the dark spots. Culture-independent approaches including scanning electron microscopy with energy dispersive X-ray spectroscopy (SEM-EDS), micro-X-ray diffraction and real-time quantitative polymerase chain reaction (qPCR) analysis were used in this study. SEM and qPCR data demonstrated that the main agents of fresco biodeterioration were mycelial fungi, with bacteria unlikely to play a major role in the development of the dark spots. SEM-EDS results showed that fungi colonization of the dark spotted areas resulted in mechanical and chemical weathering involving dissolution of mineral components of the plaster (mainly calcite) and displacement of mineral grains, which compromise the stability of the plaster or fresco. SEM-EDS also detected fungal biomineralization of secondary mycogenic minerals: calcium malate, hydrated aluminium and ferric phosphates. Biomineralization of calcium malate by fungi, as found in this study, is a rare biogeochemical phenomenon, possibly linked to the presence of calcite and nitrogen limitation.

1. Introduction

Microorganisms, being the most ubiquitous and abundant living organisms on the planet, occur in great numbers in mineral-rich environments, including building stone and other rock and mineral-based materials in the built environment and cultural heritage such as monuments (Gadd 2017; Coutinho et al., 2015; Caneva et al., 2020), museum artifacts and specimens (Pinzari et al., 2019; Piñar et al., 2020). Bioweathering or rock and mineral decay by microorganisms occurs as a result of two synergistic groups of mechanisms: biomechanical and biochemical, where biochemical processes are considered to be much more important than mechanical biodeterioration (Money 2004; Gadd, 2010). The biochemical mechanisms may include: (1) proton- and/or ligand-promoted heterotrophic leaching, which is common in many heterotrophic microbes, including fungi, (2) chemolithotrophic leaching in some chemolithotrophic bacteria and archaea and (3) redox mobilization and immobilization of metals (Sand and Bock 1991a,b; Ehrlich 1996; Lloyd 2003; Gadd et al., 2014). All these biochemical processes may be enhanced by an additional mechanism, the metal sink, comprising accumulation, precipitation and biomineralization of mobile

* Corresponding author. Zabolotny Institute of Microbiology and Virology, NAS of Ukraine, Zabolotny Str. 154, Kyiv, 03143, Ukraine.
E-mail addresses: M.Fomina@ukr.net (M. Fomina), j.cuadros@nhm.ac.uk (J. Cuadros).

https://doi.org/10.1016/j.ibiod.2022.105486
Received 30 January 2022; Received in revised form 28 July 2022; Accepted 5 August 2022
Available online 5 September 2022

metal species in and/or around the microbial biomass, reducing the external metal concentration and shifting the equilibrium towards releasing more metal into solution (Burgstaller and Schinner 1993; Fomina et al., 2007; Tazaki 2013).

Frescoes and murals can be susceptible to microbial colonization leading to aesthetic and structural damage, depending on the materials used and macro- and microclimatic conditions including temperature, humidity, and exposure to light and UV radiation (Karpovich-Tate and Rebrikova 1991; Garg et al., 1995; Feng et al., 1998; Pepe et al., 2010; Pangallo et al., 2012; Ma et al., 2020). The techniques employed in ancient wall paintings have variable susceptibility to microbial attack, depending to a great extent on the presence of organic matter used as binder for the applied mineral colors, derived either from plants (e.g., starch, gums, oils or other extracts), or animals (casein from milk, egg yolk and other gelatinous substances). The true fresco (or buon fresco) technique used coloured mineral powders mixed with lime or pure water as a painting medium that was applied to a wet lime plaster, where calcium carbonate, which is formed at the contact with air, consolidates the pigments in the wall. Thus, true frescoes lacking organic substances are regarded as more durable and less susceptible to microbial biodeterioration (Milanesi et al., 2006).

However, fungi and bacteria can attack both the inorganic and organic components of frescoes, causing efflorescence, cracks due to expansion, detachment and flaking of the outer layers, discolouration and disfiguring stains (Pinna 2021). Mechanisms of such biodeterioration are calcite dissolution, casein hydrolysis, secretion of pigments, acids, alkalis and enzymes (Pangallo et al., 2012; Unković et al., 2018). Fungi in particular can produce several coloured compounds that are either accumulated in the cytoplasm, in the cell walls or excreted (Kalra et al., 2020). Melanin is a dark-brown to black pigment, typical of some fresco-defacing fungi, and produced by oxidative polymerization of phenolic compounds (Unković et al., 2018). Other types of yellow to dark orange/brown fungal pigments (e.g., anthraquinones such as questin and asperflavin), typical of some *Eurotium* species, have also been found in fungal stains (Melo et al., 2019). Very often, oxalate patinas are produced by fungi on frescoes from calcite or metal-containing pigments in the painted layers (Gadd et al., 2014). In addition to fungi, many actinobacteria and chemoorganotrophic bacteria can produce extracellular pigments capable of causing disfiguring stains and discolouration in wall paintings (Elhagrassy 2018). Pink patinas and pink, yellow or orange discolourations on some wall paintings are caused by carotenoid pigments secreted by bacteria and algae (Nugari et al., 2009). Often, ecological succession of deteriorating agents is observed on frescoes and other painted walls, where different species alternate on the same surface, such as in the Lascaux cave, where *Chlorophyta* green algae were succeeded by two fungal species, one of them forming conspicuous and disfiguring dark melanine spots (Bastian et al., 2010).

The unique murals made using the true fresco technique in the 11th century Saint Sophia's Cathedral in Kyiv, Ukraine, which is included in the UNESCO World Heritage List, have recently suffered from dark-spot biodeterioration. Understanding the nature of wall painting deterioration, including the biogeochemical mechanisms and the groups of microorganisms involved, is essential for combatting microbial invasion and devising conservation methods. This study focused on the analysis of the dark areas that disfigure the frescoes. Scanning electron microscopy coupled with energy dispersive X-ray spectroscopy (SEM-EDS) was used to visualize the surface of the damaged areas, investigate their chemical modifications and evaluate the involvement of microorganisms in the process of stain formation. Real-time quantitative polymerase chain reaction (qPCR) analysis was used to screen the type of microorganism causing deterioration. Micro X-ray diffraction (μXRD) was used to determine the mineralogical modifications within affected areas.

2. Materials and methods

2.1. Description of the study site and sampling procedures

The main part of National Reserve "Sophia of Kyiv" (Kyiv, Ukraine) and one of the most prominent symbols of the capital of Ukraine, Saint Sophia's Cathedral (50°27′10.001″N 30°30′51.998″E) was built in ancient Kyiv in the first half of the 11th century (Fig. 1a). As one of the few surviving religious buildings of this period in Kyivan Rus, it is a monument of national significance in Ukraine, where Byzantine architectural style, mosaics and true (buon) frescoes of the 11th c. are combined with Baroque architecture and oil wall paintings of the 18th – 19th centuries.

The microclimatic conditions in the cathedral have been controlled manually for many decades (from some time in the 1950s), with the aim of maintaining the indoor air temperature within the range 14–16 °C in winter and 20–22 °C during the summer, and the relative humidity not exceeding 55%. In reality the relative humidity may vary from 35 to 46% in winter to 46–58% in summer. Currently, an automated system for microclimatic control is being developed in the cathedral.

From 2010, dark spots began to develop (Fig. 1b–e), starting on one area of the frescoes and then spreading further in the frescoes and to the restoration plaster, which was applied in the 1950s to fill gaps where the original ancient frescoes were lost (Fig. 1d). Currently, they are still slowly spreading. The dark brown spots are irregular in shape, with size varying from 100 μm up to 1 cm, although in severely affected areas the size can reach several centimeters. One part of the cathedral most affected by biodeterioration is Saint Michael's Altar, which was designated for sampling in this study (Fig. S1). All sampling processes were carried out under stringent control and the technical assistance of the restorers of the National Reserve "Sophia of Kyiv". The wall areas with restoration plaster at Saint Michael's Altar served as a model for studies of deterioration of the original frescoes. The restoration plaster is pale ochre in colour, on which background dark staining is clearly visible. Although detailed records of its composition have not survived, calcite, sand filler and some resin reinforcement (polychlorinated biphenyl or/and poly (butyl methacrylate) are believed to have been used (personal communication from curatorial team).

Sampling was carried out in the least invasive way possible and avoiding damage to the artistic content of the fresco. There were two sampling approaches, both using a sterile scalpel. First, pieces were obtained in 2018–2019 for microscopy, chemical and X-ray diffraction analyses. Five pieces (approx. size 2.5–3.5 cm) with dark spots and undamaged surface between them were collected from several areas of the restoration plaster at the Western wall of Saint Michael's Altar (Figs. S1b–e). In addition, one small piece of the damaged original fresco with red pigment on the surface (approx. size 1–1.5 cm), also from the same Western wall, was provided by the restorers (Fig. S1f). The areas without dark spots served as an undamaged control on the fresco. These collected samples were then cut into smaller pieces to be used in the several analyses. In the second sampling approach, powder scrapings were obtained for DNA extraction and qPCR. In 2019, both the Western (Figs. S1b–f) and Eastern (Fig. S1g) walls were sampled for qPCR, taking one sample of damaged areas from each wall and a single sample of undamaged plaster from the Eastern wall.

2.2. Microscopic observations and microanalysis

Following light microscopic observations of the samples, SEM coupled with EDS were used to analyse the nature of dark spot deterioration. A Tescan Mira 3 LMU microscope was used for high vacuum mode SEM observation of air-dried samples (approximately 1.0–1.5 cm in diameter) coated with 30 nm Au/Pd using a Gatan Pecs 682 sputter coater. Examination of biological structures in their pristine condition on uncoated plaster samples was performed using a variable pressure SEM (EVO50, Carl Zeiss AG, Germany) equipped with detectors for

Fig. 1. (a) A current view of St. Sophia's Cathedral, 11th c., Kyiv, Ukraine; (b–e) dark spot deterioration on the medieval frescoes on the cathedral walls; (d) spread of dark spots on areas of the frescoes (fr) and restoration plaster (rp) shown with white arrow; (e) a detailed view of the right, bottom corner of (b).

backscattered electrons (BSE) and secondary electrons (SE). The EVO50 was fitted with a tungsten filament and operated at an average working distance of 12.5 mm, and with a chamber pressure between 30 and 150 Pa, chosen according to the need for maintenance of biological structural integrity. EDS microanalysis calibration used standards ($CaCO_3$, SiO_2, albite, MgO, Al_2O_3, GaP, FeS_2, wollastonite, MAD-10 feldspar, Ti and Fe, supplied by Agar Scientific Ltd, Essex, UK) and conventional ZAF correction (for atomic number Z, absorption and fluorescence) was applied from the Oxford INCA 250 microanalysis software used for the analyses. Microscopes were operated at an accelerating voltage of 10 kV for high vacuum SEM imaging, 20 kV for ESEM imaging, and 10–20 kV for EDS. The EDS analyses were carried out in single points with the exeption of six rectangles of 13–24 μm × 10 μm, covering either an accumulation of hyphae or clusters of precipitates (see below). A total of 72 EDS analyses, including the above six rectangular areas, were used in the chemical characterization of the several types of mineral grains and biological structures observed.

2.3. Micro-X-ray diffraction (μXRD) analysis

Samples in the centimeter to millimeter range were placed on a specimen holder mounted on the XY stage of a Rigaku D/max Rapid II X-ray diffractometer. This apparatus can investigate areas of diameter as small as 30 μm in order to resolve areas of contrasting appearance on the sample surface and investigate their mineral content. The apparatus is equipped with a Cu X-ray source, a carbon monochromator and a 2D curved image plate detector. Operating conditions of the X-ray source were 40 kV and 36 mA. The samples were analyzed at an incident angle between the X-ray beam and sample surface of 7°. During the measurements, the sample was rotated around the axis perpendicular to the sample surface. The data collection time varied between 30 and 60 min and measured two-dimensional XRD patterns were converted to one-dimensional patterns using the 2DP software from Rigaku.

A total of 17 different sites in 6 different samples of restoration plaster and 6 sites in one sample of the original fresco were investigated. Colonized and uncolonized areas were readily distinguished due to the dark stains on the former. One appropriate spot was selected for each site and the X-ray beam focused on it. The sample was then rotated in order to obtain as much information as possible from the irradiated area (diffraction from the largest possible number of mineral grains and from all their available orientations).

After the analyses were performed, mineral identification was carried out using Highscore software (Panalytical) in combination with the PDF-4 database. Due to the low concentration of most mineral phases and the specific characteristics of μXRD, the relative intensity of the XRD peaks may be altered in the experimental patterns. In addition, because the analyzed surface is never flat, some peaks may appear slightly displaced from their correct position. However, mineral phase identification was aided by the numerous spots investigated.

2.4. DNA analysis

2.4.1. DNA extraction

Total DNA was extracted from 200 mg of powdered scrapings of the restoration plaster from biodeteriorated and undamaged control areas using a QIAamp DNA Mini Kit (QIAGEN) with preliminary sample treatment in Inhibitex Buffer (QIAGEN) for 10 min at 90 °C to remove inhibitors and enable amplification with high sensitivity. Standard samples of fungal and bacterial DNA for qPCR were obtained from biomasss (200 mg) of pure cultures of *Saccharomyces cerevisiae* UCM Y-

527 and *Escherichia coli* UCM B-906 (Ukrainian Collection of Microorganisms, Zabolotny Institute of Microbiology and Virology of NAS of Ukraine) also using a QIAamp DNA Mini Kit (QIAGEN). Three replicates of every collected sample were analyzed. The quality and quantity of extracted DNA samples were determined using a NanoDrop ND-1000 spectrophotometer.

2.4.2. Quantitative Real-Time PCR (qPCR)

Fungal total DNA was amplified using primers for fungal 28S rRNA gene region: 28s-f 5′-ATATCAATAAGCGGAGGAAAAG-3′ and 28s-r 5′-ATTCCCAAACAACTCGACTC-3' (Bates and Garcia-Pichel 2009). Similarly, bacterial DNA contamination was analyzed using primers for the 16S rRNA gene locus: 16s-f 5′-ACTCCTACGGGAGGCAGCAG-3′ and 16s-r 5′-ATTACCGCGGCTGCTGG-3' (Fierer et al., 2005). The qPCR was performed using a CFX96 Real-Time PCR System (BIORAD) with 2x Universal SYBR Green Supermix SsoAdvanced (BIORAD) according to the manufacturer's instructions with some slight modifications: each qPCR reaction was performed in a total volume of 15 μl containing 5 μl of DNA template, 1 μl of 10 μM fungal or bacterial primers, 7.5 μl of SYBR Green mix and 1 μl of 25 mM $MgCl_2$. The thermal cycling PCR conditions consisted of an initial denaturing and polymerase activation step at 95 °C for 3 min, followed by 35 cycles of 95 °C for 15 s (DNA denaturation step), 55 °C for 30 s for bacterial primers or 59 °C for 40 s for fungal primers (primer annealing step), and of 72 °C for 30 s (DNA elongation step). The fluorescence reading was performed after the DNA elongation step. A melt curve analysis was carried out by increasing the temperature from 54 °C to 90 °C in 0.5 °C steps to detect target PCR-fragment amplification as well as primer dimers and unspecific amplicons.

Similar to the approach used by Liu et al. (2018), fungal and bacterial DNA concentrations in deteriorated and undamaged plaster samples were quantified using standard curves. DNA of *E. coli* and *S. cerevisiae* were chosen as the external standards for bacterial and fungal DNA, respectively, in a 5- and 10-fold dilution series, respectively. The standard curve was constructed by plotting logarithmic values of the serial dilution of standard samples with defined DNA concentrations in double replicates versus the threshold cycle (Ct) values generated from qPCR.

2.4.3. qPCR quantification of rDNA genes

The quantificaton of rDNA genes was aimed to establish the type of microrganisms acting as biodeteriorative agents of the frescoes, fungi and/or bacteria. The number of copies of rDNA genes per genome varies between different microbial species, strains within species and depends on environmental conditions, level of nutrition, transcriptional activity and stress factors (Kwan et al., 2016; Kobayashi and Sasaki 2017). The genome size in fungi can vary between 15.8 and 49 Mbp, and the rDNA gene copy number ranges from 14 to over 250 (Salim et al., 2017). In contrast, these indicators vary in a much smaller range in bacteria (Fogel et al., 1999). Due to the large variability in genome size and the number of rDNA copies per genome in prokaryotes and fungi, and the different size range, absolute quantification of microbial biomass in environmental samples using qPCR is complicated and poorly standardized. To overcome this limitation, the alternative approach was employed of using the standard genomes of model microorganisms and separate genetic markers specific for bacteria and fungi for the comparative evaluation of the bacterial and fungal rDNA in the plaster. The microbial quantification was compared with genomic DNA isolated from standard pure cultures of typical fungal and bacterial species *Saccharomyces cerevisiae* (~150 rDNA copies per 12 Mb genome; Kwan et al., 2016) and *Escherichia coli* (7 rDNA copies per 4.6 Mb genome; Fogel et al., 1999), respectively. We estimated the number of genomes from the formula

$$\text{Number of genomes} = \frac{\mathbf{X}(\text{ng}) \times 6.0221 \times 10^{23}\left(\frac{\text{molecules}}{\text{mole}}\right)}{\mathbf{G} \times \mathbf{C} \times 660\left(\frac{\text{g}}{\text{mole}}\right) \times 10^{9}\left(\frac{\text{ng}}{\text{g}}\right)}$$

where X is the amount of fungal or bacterial DNA in our samples obtained by qPCR, G is the size of the standard genome for *E. coli* and *S. cerevisiae*, C is the number of copies of target gene per standard genome, and 660 g/mol = average mass of 1 bp dsDNA. We assumed that each typical bacterial and fungal cell was haploid.

2.5. Statistical analysis

EDS measurements were analyzed using one-way analysis of the variance (ANOVA) at 95% confidence to evaluate relationships between the variables (measured elements), and the significance of the differences between specific areas within each sample. The ANOVA model used was "unbalanced" because the number of observations within each category was not the same. ANOVA was followed by a Tukey's Honest Significant Difference test, a post-hoc test based on the studentized distribution range. Principal Components Analysis (PCA) was used to visualize the correlations between all the variables (Massart et al., 1998) and reduce the number of variables for further statistical analysis. The factor scores obtained for the first four principal components (PCs) resulting from PCA were then used to run Discriminant Analysis (DA). The DA was carried out with four variables (the first four PCs). The step of reducing the number of variables was necessary to perform the DA because this analysis requires 3 to 20 times as many samples as variables (Massart et al., 1998). ANOVA, PCA and DA analyses were performed using XLSTAT 2019.3.2 software (Addinsoft, 2021).

3. Results

3.1. SEM(ESEM)-EDS examination of deteriorated areas with dark spots

SEM observations of the areas with dark spots on the restoration plaster revealed the microbial nature of the deterioration as there were abundant fungal hyphae within a disturbed plaster surface (Figs. 2 and S2). However, no signs of bacterial growth were observed with high-resolution SEM imaging (Fig. S3). It was evident that the integrity of the mineral matrix was compromised at the biodeteriorated sites because the surface was loose, with obvious spalling and cracking, and colonized by fungal hyphae that penetrated holes and cracks (Fig. S2). Environmental SEM observations also revealed the dense subsurface aggregates of fungal mycelium causing mineral matrix expansion (Fig. 2a). Numerous particles such as flake-like aggregates and calcium-rich crystals of distinct morphology were closely associated with fungal mycelium, probably a result of biogeochemical activities of the colonizing fungi (Figs. 2 and S3).

Multiple EDS analyses were obtained from biodeteriorated areas covered with fungal mycelium (F), associated flake-like precipitates (X) and calcium-rich crystals (C) as well as surrounding control areas (B) (Figs. 2 and S3; Table 1). Magnesium was high in both (B) and (X) (0.17–0.14% atoms, Table 1), possibly indicating the presence of a carbonate (Mg or Ca–Mg carbonate) in the plaster (as previous to contamination; termed background hereafter, for simplicity) and precipitates. Silicon was lowest in (C), indicating that most of the analyzed crystals were not silicates. Calcium was high (5.63–9.57% atoms, Table 1) in all types of particles indicating one or several Ca-containing phases (carbonate, gypsum, or calcium associated with low molecular weight organic acids produced by fungi) were present in all types of areas investigated. Statistical analysis (ANOVA) of elemental composition data indicated that only Na, Cl and Ti were not significantly different between the several types of targets analyzed (B, X, F and C; Table 1, last column). In other words, the different morphologies observed had significantly different chemical compositions.

PCA was used to investigate the systematic variations between the analyzed elements in the dataset. Fig. S4 shows the correlation circle obtained on the first two coordinates F1 and F2 (Fig. S4A) and a projection of all the variables on the plane generated by factors F1 and F2 (Fig. S4B). The two coordinates (or the first two principal components)

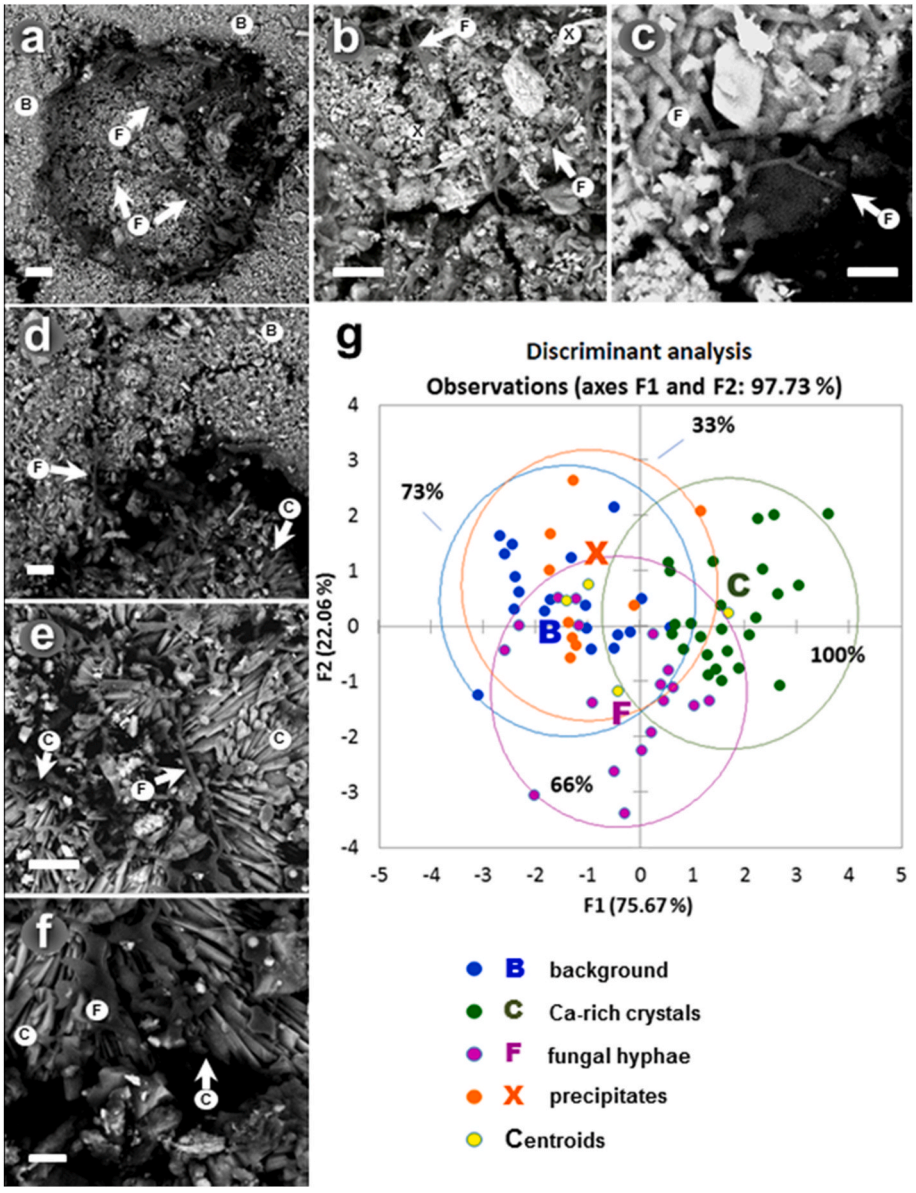

Fig. 2. Areas with dark spots on the restoration plaster examined by low-vacuum mode SEM coupled with energy dispersive X-ray spectroscopy (ESEM-EDS): (a–f) ESEM micrographs (typical images) featuring heavily deteriorated areas with abundant fungal hyphae, and associated with fungal flake-like precipitates (b) and calcium-rich crystals (d–f); (g) plot of the discriminant analysis (DA) of element concentration distribution in the different sites of EDS examination. Letters in the circles in (a–f) denote: (B) sites of background without visible deterioration, (C) calcium-rich crystals, (F) fungal hyphae and (X) other precipitates. Scale bars: (a, b, e) 20 μm; (c, d, f) 10 μm.

F1 and F2 explain 57.83% of the total variance of the dataset. Based on the percentage contribution of the individual variables to the new components and the correlation values obtained between the variables and the factors (data not shown), the first component was related to the concentration of most elements, Mg, Al, Si, P, K, Fe and Zn. Because Mg is grouped with these elements, it is possible that most Mg is contained in silicate minerals rather than in carbonates, as initially considered. The second component was mainly related to oxygen and accounted for 14.16% of the variance, while the third principal component (not shown in Fig. 4S) was related to the presence of Ca and S and accounted for 8.62% of the variance. Variables (the chemical elements, represented by the vectors) that are far from the centre, close to each other and forming an acute angle, have a significant positive correlation (r is positive and high). Variables far from the centre, on opposite sides, and therefore forming an obtuse angle, have a significant negative correlation (r is negative and high). Variables at right angles from each other are not correlated (r close to 0).

Chemical values (Table 1) and PCA results indicated that: (i) the crystals in close proximity to the fungal biomass possessed high Ca and C content (all columns, Table 1), but these two elements were negatively correlated with each other (Fig. S4), which means that other components in the background have still higher C and/or Ca (minerals from B contaminate analyses from X, F and C in different extents); (ii) S was mostly low (Table 1) and independent from Ca (Fig. S4), indicating that the abundant precipitated Ca-rich crystals were not gypsum; and (iii) there were several silicate minerals in the plaster that contained mixtures of Si, Al, Fe, Mg, K and Zn.

Using PCA analysis, a new system was generated with the principal components (or coordinates) where the chemical results were investigated in terms of the type of changes induced by fungal activity on the fresco or restoration plaster. For this, the scores of the chemical values in the new system were analyzed using discriminant analysis (DA) to model a set of linearly independent variables capable, if possible, to predict the group to which each variable belongs. Because the principal components (F1, F2, … *Fn*) are linearly independent by definition, they provide a suitable variable set for group identification. In this investigation, the cumulative variability of the first four components from the PCA analysis accounted for 73.53% of the variance of the whole dataset.

The DA (Fig. 2g) showed that chemical results can discriminate between the four types of analyses identified visually during SEM investigation (B, F, C and X), confirming results from ANOVA analysis. The DA plot shows two complementary results. One is the confidence ellipse

Table 1
Element distribution in the areas of dark spot-biodeterioration, from samples of restoration plaster and fresco, as examined with Environmental SEM-EDS. Four types of areas are discriminated: (B) background or plaster with no signs of fungal activity or deterioration; (X) flake-like precipitates; (F) fungal hyphae and (C) calcium-rich crystals. Values correspond to atomic % after normalization to 100%, and are the means from a minimum of 10 replicates. Means in a column without a common letter (a/b) differ for $P < 0.05$, as analyzed by one-way ANOVA and Tukey's *post hoc* test.

Elements	Sites of EDS examination				*P*	Significant
	B	X	F	C		
C	35.36 *b*	33.12 *b*	46.35 *a*	39.98 *b*	*<0.0001*	Yes
O	49.83 *ab*	51.88 *a*	43.45 *c*	46.58 *bc*	*<0.0001*	Yes
Na	0.9 *a*	0.04 *a*	0.09 *a*	0.05 *a*	*0.32*	No
Mg	0.17 *a*	0.14 *ab*	0.07 *bc*	0.02 *c*	*<0.0001*	Yes
Al	1.44 *a*	1.09 *ab*	0.77 *b*	0.73 *b*	*<0.0001*	Yes
Si	2.89 *a*	2.62 *ab*	2.13 *ab*	1.75 *b*	*0.00*	Yes
P	0.19 *a*	0.11 *ab*	0.08 *b*	0.04 *b*	*<0.0001*	Yes
S	0.76 *ab*	1.26 *a*	0.54 *ab*	0.31 *b*	*0.02*	Yes
Cl	0.15 *a*	0.14 *a*	0.16 *a*	0.12 *a*	*0.84*	No
K	0.25 *a*	0.23 *ab*	0.16 *b*	0.18 *ab*	*0.01*	Yes
Ca	7.79 *ab*	8.47 *a*	5.63 *b*	9.57 *a*	*<0.0001*	Yes
Ti	0.01 *a*	0.01 *a*	0.01 *a*	0.00 *a*	*0.78*	No
Fe	0.97 *a*	0.82 *ab*	0.51 *b*	0.63 *b*	*0.00*	Yes
Zn	0.08 *a*	0.10 *a*	0.06 *ab*	0.02 *b*	*0.00*	Yes

for each group with the corresponding centroid (the group centroid is the mean value of the discriminant score for a given category of the dependent variable). The ellipses are meant to include the maximum number of data points of each group while containing the minimum possible number of results from other groups. The other result is the percentage of data (Fig. 2g, percent values) successfully classified into each group (*i.e.*, falling into the group originally assigned to them) according to the confusion matrix. The most successful classification was that of the Ca-rich crystals (C) with 100% of the data correctly assigned, followed by the background (B, 73%), the fungus (F, 66%) and the flake-like and other precipitates (X) that were poorly classified by the analysis (33%). These results are meaningful because the F and X categories represent the objects with lower apparent density (Fig. S3) and thus their analysis should have been more significantly contaminated by categories C and B (lower density means deeper penetration of the electron beam and higher chances of contamination with other particles below).

Considering that the Ca-rich crystals (C) observed on the plaster samples may also contain attached fungal hyphae and their extracellular metabolites (e.g., EPS) as well as other smaller mineral particles, this could probably lead to a modified stoichiometry when examined by EDS. We however averaged all our EDS data for Ca, C and O content in these crystals, which produced the Ca:C:O stoichiometry of 1:4.2:4.9, which is very close to the values for Ca malate ($CaC_4H_4O_5$) of 1:4:5.

3.2. μXRD analysis of mineral phases

To identify the precipitates and crystals found in the zones affected by fungi, a μXRD study was performed on undamaged control restoration plaster and original fresco, and on the areas with dark-spot deterioration of both the restoration plaster and fresco (Table 2; Fig. 3). It was revealed that three mineral phases were present in the majority of areas affected by fungal growth on both restoration plaster and the original fresco, and only appeared in the colonized areas, indicating that they were precipitated as a result of fungal activity. Two of the minerals precipitated by fungi, Ca-malate (also confirmed by stoichiometric analysis of the Ca-rich crystals precipitated by the fungus obtained from SEM-EDS data) and a hydrated Al-phosphate ($AlPO_4 \cdot 1.67H_2O$), showed XRD peaks at a low angle that were readily identified. The third mineral phase, strengite ($FePO_4 \cdot 2H_2O$), was more difficult to identify as only one intense peak occurred at 4.39 Å (20.2 °2θ) (Table 2; Fig. 3a,c).

The restoration plaster and the original fresco plaster were very similar in their mineral composition. They consisted of calcite as the main component, followed by quartz and a group of other minerals in minor to trace concentrations (Fig. 3, Table 2). The lack of identification of specific mineral phases does not necessarily mean lack of their presence because some peaks may have been masked by those of other minerals. For example, cristobalite was identified only in a few spots (Table 2), but it may have been present more widely since its only intense peak (4.10–4.08 Å, 21.6–21.8 °2θ) overlapped with those of other phases in higher concentrations (e.g., Ca-malate and enstatite) (Fig. 3). The only difference between the restoration plaster and the original fresco sample was the presence of hematite in the fresco (Table 2, Fig. 3).

Several mineral phases corresponded to minerals with compositional solid solutions and thus exhibited different XRD patterns. This was the case with albite ($NaAlSi_3O_8$) and microcline ($KAlSi_3O_8$), where compositions ranged between the Na and K end-members, although Na-rich compositions were more frequent. The pyroxenes presented a range of compositions between the Mg end-member (enstatite $Mg_2Si_2O_6$) and intermediate compositions (augite Ca [Mg,Fe,Al][Si,Al]$_2O_6$), with one case of the Ca–Fe end-member (hedenbergite $CaFeSi_2O_6$). The amphiboles also corresponded to several compositions of the hornblende series ([Na,Ca]$_2$ [Mg,Fe,Al]$_5$ [Si,Al]$_8O_{22}$ [OH]$_2$). Such mixed compositions within hand specimens are common in all the above mineral groups. The assignment of andradite was based on its most intense peak at 2.70 Å (33.2 °2θ). This peak overlapped with peaks from other minerals, but either the centre of the peak or a shoulder was most frequently coincident with that of andradite (Fig. 3).

It should be also noted that light microscopic observations made during μXRD analyses revealed numerous small black particles (approx. size ≤50 μm) that were present in both the original fresco and restoration plaster. These black particles were not of mineral nature and did not produce diffraction patterns. They were not recognized during the SEM-EDS investigation. We find two possible origins for these particles. One is char mixed in the plaster, a common historical procedure (Barrett et al., 2020). The other is a possible natural or man-made resin reinforcement used in the plaster.

3.3. qPCR evaluation of fungal and bacterial biomass in the dark spots

The *S. cerevisiae* and *E. coli* standard curves for fungal and bacterial biomass showed correlation coefficients >0.91 and a qPCR efficiency of approximately 100% (Fig. 4b,d). Fungal abundance in the areas with dark spots were high, whereas the fungal rDNA amount in the control samples was below detection levels, not reaching the threshold line on the amplification curves for fungi (Fig. 4c, Table S1). Thus, only a negligible quantity of fungal biomass was present on undamaged walls. In contrast, the bacterial biomass in control samples was within the range found in biodeteriorated spots (Fig. 4a, Table S1). Thus, our qPCR study demonstrated that bacterial DNA concentrations were not correlated with the investigated areas being undamaged or biodeteriorated, while fungal DNA was present only in the sites of biodeterioration. Microbial populations varied between the two sampled walls. In particular, fungal concentration on the Eastern wall of Saint Michael's Altar was almost 25 times that of the Western wall.

4. Discussion

4.1. Mineral composition of the original fresco and restoration plaster in St. Sophia's cathedral

This research has revealed the microbiological nature of dark-spot biodeterioration of medieval murals in St. Sophia's cathedral. It is known that the biodiversity of microorganisms colonizing art works strongly depends on the chemical composition of the substrate and the conditions of the surrounding microenvironment (Ciferri 1999). In our

Table 2
Mineral composition of the surface of samples examined with μXRD.

		Minerals*													
#	Sample	1	2	3	4	5	6	7	8	9	10	11	12	13	14
1		X	X		X	X	X		X			X			
2	**Restoration**	X	X	X	X	X	X		X			X			
3	**plaster**	X	X	X	X	X	X		X			X			
4	**control**	X	X	X	X	X	X		X	X					
5		X	X	X	X		X		X	X					
6		X	X	X	X		X		X	X					
7	**Fresco**	X	X	X	X		X		X		X				
8	**control**	X	X	X		X	X			X		X			
9		X	X	X	X	X	X		X				**X**	**X**	
10		X	X	X			X		X				**X**		
11		X	X	X	X	X	X		X				**X**	**X**	
12	**Dark spots on**	X	X	X	X		X		X				**X**	**X**	**X**
13	**restoration**	X	X	X	X	X	X		X	X			**X**	**X**	**X**
14	**plaster**	X	X	X	X	X	X		X	X			**X**	**X**	**X**
15		X	X	X	X		X		X	X			**X**	**X**	**X**
16		X	X	X	X		X		X				**X**	**X**	**X**
17		X	X	X	X		X		X				**X**	**X**	**X**
18		X	X	X	X		X		X				**X**	**X**	**X**
19		X	X	X	X		X	**X**	X	X			**X**	**X**	**X**
20		X	X	X	X			**X**		X	X	X	**X**	**X**	**X**
21	**Dark spots on**	X	X	X	X		X	**X**	X	X	X		**X**	**X**	**X**
22	**fresco**	X	X	X	X				X	X	X		**X**	**X**	**X**
23		X	X	X	X		X	**X**	X			X	**X**	**X**	

X – indicates presence of mineral.
Bold **X** – indicates mineral presence only in dark spots.

*** Minerals:**
1 – Calcite [$CaCO_3$]; **2** – Quartz [SiO_2]; **3** – Gypsum [$CaSO_4{\cdot}2H_2O$]; **4** – Albite [$NaAlSi_3O_8$]; **5** – Microcline [$KAlSi_3O_8$]; **6** – Pyroxenes: Augite [$(Ca,Na)(Mg,Fe,Al,Ti)(Si,Al)_2O_6$], Enstatite [$Mg_2Si_2O_6$], Hedenbergite [$CaFeSi_2O_6$]; **7** – Amphiboles: Hornblende [$(Ca,Na)_2(Mg,Fe,Al)_5(Al,Si)_8O_{22}(OH)_2$]; **8** – Garnet group: Andradite [$Ca_3Fe_2Si_3O_{12}$]; **9** – Eugsterite [$Na_4Ca(SO_4)_3{\cdot}2(H_2O)$]; **10** – Hematite [$Fe_2O_3$] (present only on fresco); **11** – Cristobalite [SiO_2]; **12** – Ca-malate [$CaC_4H_4O_5$]; **13** – Hydrated Al-phosphate [$AlPO_4{\cdot}1.67H_2O$]; **14** – Strengite [$FePO_4{\cdot}2H_2O$].

nn. 7 and 20-22 are sites on the side of the fresco surface; 8 and 23 are analyses on the back of the sample (or side opposite to the fresco surface).

work, the mineral composition of the frescoes and restoration plaster and the specific microclimate of the cathedral are two very important factors defining the microbiota of dark spotted areas.

Calcite was the most abundant mineral in restoration plaster and fresco, and is the intended product of plaster preparation. Hematite was only present in the original fresco because this was used as red pigment by the medieval artists. All other minerals present were common to the original fresco and restoration plaster. It was surprising that the minor components of both the restoration plaster and the fresco mineral matrix, prepared and applied with a difference of nine centuries, were approximately the same. Quartz and the albite-microcline feldspar series have probably the same origin as the sand that was either present in the original limestone that was used or mixed with it later. Cristobalite may have been a component of this sand or a product of partial dissolution of one of the above phases in the highly alkaline environment of the wet plaster (Ca $[OH]_2$), followed by precipitation of the cristobalite. Gypsum ($CaSO_4{\cdot}2H_2O$) and eugsterite (Na_4Ca $[SO_4]_3{\cdot}2H_2O$) may be reaction products after application of the plaster. The pyroxenes, amphiboles and andradite ($Ca_3Fe_2Si_3O_{12}$) probably have a common origin. They may have been present in the sand mixed with the quarried calcite. This shows that the sand contained minerals with different origins, both felsic (quartz and Na–K-feldspars) and mafic (pyroxenes and amphiboles). Andradite may have also been part of the limestone used if it had been partially metamorphosed mixed with silicates.

4.2. Mechanisms of fungal transformation of mineral substrata in the biodeteriorated areas of the cathedral walls

The SEM images revealed abundant fungal mycelium colonizing the wall surface. Consideration of the local low humidity (35–58%) maintained in the cathedral makes it likely that these fungi are xerotolerant or/and xerophilic (Sklenář et al., 2017). Such fungi are able to produce a variety of coloured pigments ranging from dark-orange to brown and black (Visagie et al., 2017; Lagashetti et al., 2019), which would cause

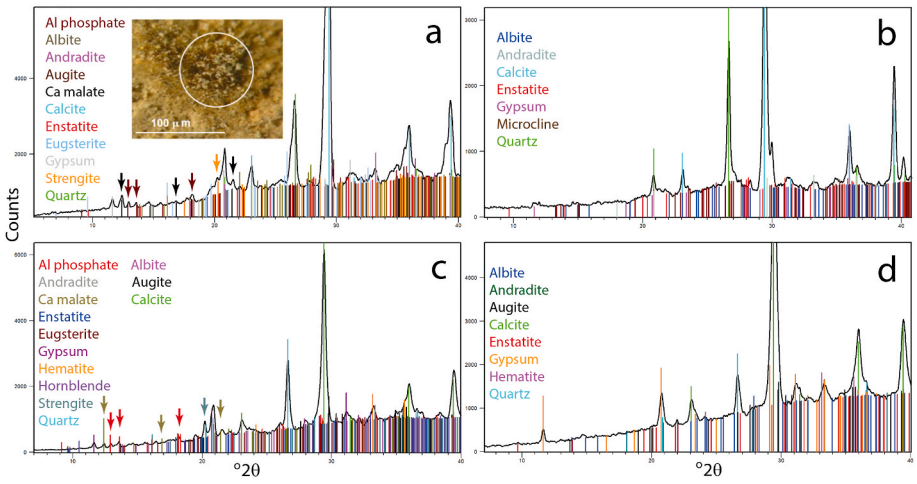

Fig. 3. Typical X-ray diffraction (XRD) patterns and mineral phases from deteriorated areas with dark spots (a, c) and undamaged control areas (b, d) on restoration plaster (a, b) and the original fresco (c, d). The position of the XRD peaks of the identified minerals are shown by the lines, where colors correspond to that of the mineral indicated. Arrows indicate the position of peaks important for the identification of minerals precipitated by fungi. The low-angle areas below 10 °2θ in the X-ray patterns are unreliable because the diffracted X-ray beam is liable to be cut-off by irregularities on the sample surface. The inset photograph (a) shows one of the dark spots with white crystals precipitated by fungi on restoration plaster (μXRD was performed within the circle).

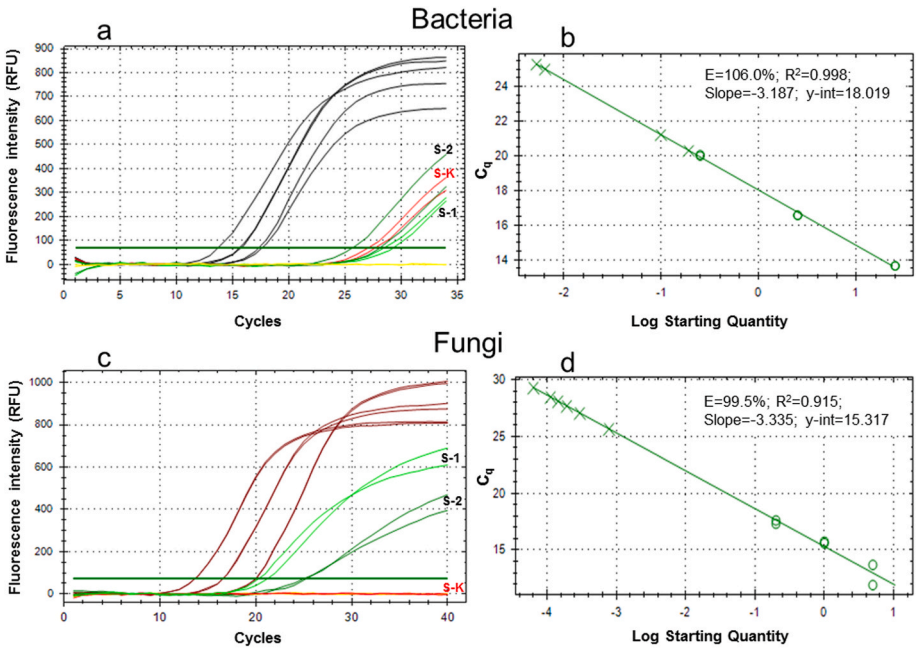

Fig. 4. Quantitative Real-Time PCR (qPCR) amplification curves (a, c) and quantification cycle (Cq) standard calibration curves (b, d) for microbial biomass of bacteria (a, b) and fungi (c, d). *E. coli* standard amplification curves are shown in black (a); *S. cerevisiae* standard amplification curves are shown in brown (c). In a and c, the microbial biomass in dark spot samples are from the Eastern (S-1, light green) and Western (S-2, darker green) walls of St. Michael's Altar, and the control, unstained samples are the S–K lines (red); the no template control (NTC) is shown in yellow. Dark green straight horizontal lines are amplification threshold lines. In b and d, the circles show values from standards of microbial biomass and crosses depict the studied samples from wall scrapings; the qPCR efficiency (E) and parameters of the linear regression equations (R^2, slope and y-intercept) are shown in the plots.

staining and disfiguration of the wall paintings (Fig. 1). Along with purely aesthetic consequences, many other fungi can cause severe structural damage of wall paintings, including cracking and disintegration of paint layers (Ciferri 1999). For the true (or buon) fresco in St. Sophia cathedral, structural damage is clearly a result of biogeochemical activities of the microbiota in the dark-spotted areas. As visualized by SEM, fungi thrived on the restoration plaster and frescoes and significantly compromised the integrity of its mineral matrix (Figs. 2 and S2). Biochemical attack on the mineral matrix by fungal excretion of protons and metabolites was evident by the massive precipitation on the fungal hyphae which could be easily observed by light microscopy. Biochemical mechanisms in mycelial fungi are usually accompanied by biomechanical disruption of minerals occurring through direct hyphal penetration into decayed mineral matrix along crystal planes, cleavage, cracks and grain boundaries (Banfield et al., 1999; Kumar and Kumar 1999; Sterflinger 2000). Such penetration may be facilitated by thigmotropic (or contact guidance) reactions and lubrication with extracellular polymeric substances (EPS) that may contain acidic and metal-chelating metabolites (Gadd et al., 2014; Gadd 2017). Such reported mechanisms were evident in our SEM observations, which showed physical detachment of plaster particles by colonizing mycelium (Fig. S3a) as well as abundant precipitates within the plaster fabric (Fig. 2e,f and Figs. S3b–g), with loss of plaster where massive precipitation occurred (Fig. 2a,d). The overall effect was increased porosity and roughness of surfaces in the dark spots compared to undamaged sites (Fig. S2).

Our chemical, mineralogical and surface morphology data of plaster and fresco provide a new insight into the mechanisms of biogeochemical processes transforming mineral substrata in medieval buon frescoes deteriorated by fungi (Fig. 5). The biogeochemical activity resulted in the formation of new mycogenic mineral phases associated with the fungal hyphae: Ca-malate, hydrated Al-phosphate ($AlPO_4{\cdot}1.67H_2O$) and strengite ($FePO_4{\cdot}2H_2O$). Such biomineralization was obviously preceded by mineral dissolution. Evidence that mineral dissolution took place includes: (i) the increased porosity in the affected plaster, (ii) the presence of Ca malate indicates secretion of malic acid or an equivalent combination of protons with partially or fully deprotonated malate (Vrabl et al., 2012), (iii) calcite is readily dissolved by acids and dissolution by malic acid produces Ca malate. Biomineralization of mobile metal species released by geoactive microorganisms and resulting in

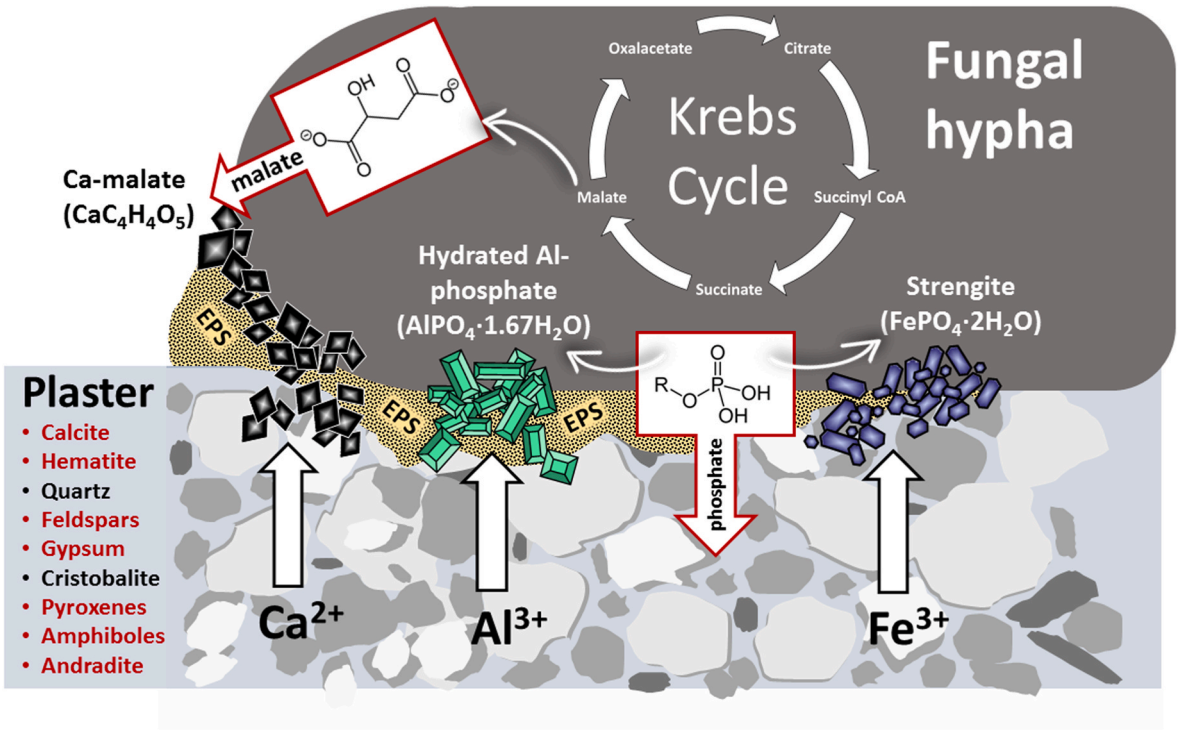

Fig. 5. Model of the biogeochemical mechanisms involved in the transformation of restoration plaster and fresco. The microenvironment of the fungal mycelium on the surface of colonized plaster consists of hyphae and extracellular polymeric substances (EPS) which retain moisture and facilitate dissolution-precipitation reactions and diffusion of metal and anionic species. Fungi biochemically attack the plaster through heterotrophic leaching by excreting protons and ligands that dissolve the plaster minerals (in red) and release chemical species that may contribute to newly-precipitated minerals. Excreted malate is shown as a side product of the Krebs cycle (tricarboxylic cycle, citric acid cycle). Phosphate may be released by phosphatase activity or acid production. Although other metal and anionic species are likely to be dissolved in the mycelium-plaster interface, the minerals precipitated are those that first reach supersaturation.

formation of secondary minerals (e.g. phosphates, carbonates, sulfides, oxides and oxalates) is a well-known phenomenon (Gadd 2010, 2017; Gadd et al., 2014). Low molecular weight organic acids (LMWOA) excreted by fungi are crucial agents of bioweathering of frescoes and other mineral-based objects of historical-cultural heritage (Gadd 2017). Many fungi isolated from biodeteriorated mural paintings in temples and tombs possess the ability to dissolve calcite through production of LMWOA (e.g. citric, fumaric, lactic, succinic, acetic and oxalic acids) (Unković et al., 2018; Ma et al., 2020). Of these, oxalic/oxalate is of principal significance because of its efficiency for mineral dissolution, metal complexation and precipitation of secondary metal oxalates, which can form in fissures and pores causing mechanical damage. For example, whewellite and weddellite (calcium oxalates) crystals have often been observed on the surfaces of limestone, sandstone, granite and plasters of historical buildings and monuments, as well as on cave paintings and indoor murals (Gadd 2017; Salvadó et al., 2016).

Despite malate being produced by all fungi as an intermediate of the citric acid cycle, fungal biomineralization of calcium malate is a much rarer phenomenon than calcium oxalate precipitation. In fact, there has been only one report of biomineralized calcium malate, found in the dark spots covering the surfaces of 14th century murals in Saint Michael's Chapel (Royal Monastery of Pedralbes, Barcelona, Spain), painted using a mixed fresco technique («a fresco+a secco») (Salvadó et al., 2016). The authors suggested that the presence of calcium malate along with other calcium salts of fumaric, oxalic or succinic acid in the sites of deterioration was directly related to the activity of fungi. Vasanthakumar et al. (2013) also reported relevant results from dark spots on the painted walls of Tutankhamun's tomb, but did not provide the composition of plaster or pigments. The spotted plaster contained 16 wt% of malic acid (as detected by gas chromatography coupled with mass spectrometry; but the exact species, malic acid or malate salt, was not identified). They did not find microbes associated with the spots but one fungus identified from cultivable isolates sampled elsewhere in the chamber, *Penicillium chrysogenum*, produced malic acid *in vitro*. They interpreted that the dark spots were caused by fungi that had died and disappeared from the damaged areas. Our work therefore reports the first complete observation and description of fungal transformation of calcite into calcium malate in restoration plaster and medieval frescoes.

In liquid nutrient media, it was found that high levels of L-malate were produced by fungi under conditions of nitrogen starvation in the presence of $CaCO_3$ (Chi et al., 2016; Kövilein et al., 2020). It can be hypothesized that the abundant calcite in the frescoes of St. Sophia cathedral combined with nitrogen source limitation might create conditions favouring malate over-excretion and subsequent calcium malate biomineralization by the colonizing fungi.

The two phosphates found in the stained areas, hydrated Al-phosphate ($AlPO_4 \cdot 1.67H_2O$) and strengite ($FePO_4 \cdot 2H_2O$), are common precipitates occurring as a result of fungal activity (Gadd 2010). In the absence of phosphate minerals in the original plaster of the cathedral walls, the phosphate groups could originate both from hyphal surfaces of metabolically-active fungi and from inert organic matter, such as that after death and decomposition of fungal and bacterial cells (Fig. 5). It is known that fungi are able to precipitate metal phosphates from organic P resources through the activity of fungal phosphatases, produced extracellularly and often associated with the fungal cell wall. These enzymes hydrolyze different organic-P sources releasing inorganic phosphate (Liang et al., 2015).

4.3. *Relative contributions of fungi and bacteria to dark-spot biodeterioration*

Our data provide convincing evidence of the fungal contribution to the biodeterioration in Saint Sophia's Cathedral. Fungi can be resistant to extreme environmental conditions (temperature, desiccation,

nutrient limitation, metal toxicity, UV irradiation). Most relevant for our study, xerophilic/xerotolerant fungi are able to survive under the harsh conditions of the cathedral walls, which include extreme dryness and limited nutrient resources. Some xerophilic fungi are capable of thriving at very low water activities ($a_w \sim 0.6$), some of which are very difficult to cultivate under laboratory conditions (Liu et al., 2018). In addition, fungal pigmentation, the biogeochemical activities observed in direct connection to fungal hyphae and the ability of some fungal species to excrete malate/malic acid all point to fungi as the main agents causing the bioweathering of the mineral matrix of the walls. Generally, fungi perform mineral dissolution more efficiently than bacteria, at higher pH values and over a wide redox range (Burford et al., 2003; Gadd 2007; Knabe and Gorbushina 2018; Turnau et al., 2020).

In spite of all the positive evidence for the presence and deteriorating action of fungi in this study, and also of the negative evidence that bacterial cells and biofilms were not observed in the dark spots using SEM, it was necessary to investigate whether bacteria might also have contributed to plaster damage. Modern culture-independent molecular biology approaches have revealed a previously hidden microbial biodiversity in cultural heritage artifacts as well as the relative abundance of the several species (Michaelsen et al., 2010; Sugiyama et al., 2017; Tomassetti et al., 2017; Liu et al., 2018; Piñar and Sterflinger, 2021). For example, real-time qPCR analysis of deteriorated wood and leather artifacts in Tianjin Museum, China, suggested that microscopic fungi were more important deteriorative agents than bacteria (Liu et al., 2018).

In our study we followed the same approach as Liu et al. (2018), using 28S rRNA gene and 16S rRNA gene as genetic markers for fungal and bacterial biomass, respectively. For bacteria, where genome size and the number of ribosomal genes do not vary over a wide range, this method is rather accurate. For fungi, however, the wider range of genome size and number of ribosomal genes means that this method of quantification is approximate (Ettenauer et al., 2014). In addition, the cell walls of mycelial fungi involved in biodeterioration may differ from those of *S. cerevisiae* in density, biomechanical properties and biochemical composition, which may also include PCR inhibitors. Therefore, the efficiency of DNA extraction and subsequent PCR could vary significantly for different fungi and differ from the selected standard. Also, the variability of the qPCR data might depend on the degree of colonization of the particular sampling sites. Not only the surface area colonized by microbes is relevant to the quantification but also the microbial 3D distribution within the porous mineral matrix of the plaster (with numerous cracks, fissures, spalling, etc.), which was evident in our SEM observations.

Bacterial DNA was found in Saint Sophia's Cathedral walls, indicating the presence of bacterial cells, spores, and residues of bacterial biofilms. It is unclear whether these bacteria are physiologically active or whether they contribute to biodeterioration of frescoes. From qPCR data, however, it was demonstrated that the quantity of total bacterial DNA in the dark-spot areas did not significantly differ from undamaged control zones, whereas the presence of total fungal DNA distinctly correlated with biodeterioration sites, with control areas manifesting none or negligible fungal DNA. Thus, the potential difficulties of microbial DNA quantification discussed above did not affect this investigation. The bacteria in the cathedral walls may arise from indoor contamination related to dust and human activities, either recently or in the past.

5. Conclusions

Filamentous fungi are the main agents of dark-spot biodeterioration in St. Sophia's cathedral, Kyiv. Fungal colonization had biogeochemical consequences, compromising the integrity of the original mineral matrix of the wall surfaces. The mechanisms of mineral matrix biodeterioration included mineral dissolution and the formation of secondary mycogenic minerals: calcium malate, hydrated aluminium phosphate and ferric phosphate (strengite). Fungal precipitation of calcium malate is a rare phenomenon which has been recently linked to specific conditions of nitrogen starvation and presence of calcium carbonate. Our results may therefore corroborate that these are environmental triggers of such a rare biogeochemical process. Despite the presence of bacterial DNA in the walls of the cathedral, qPCR data for biodeteriorated and undamaged areas and SEM observations indicated that bacteria do not play a major role in the development of dark spots on the frescoes.

Declaration of competing interest

The authors declare that they have no known competing financial interests or personal relationships that could have appeared to influence the work reported in this paper.

Acknowledgements

MF and MG would like to acknowledge the partial financial support by the National Reserve "Sophia of Kyiv" (Kyiv, Ukraine) through scientific research work on the economic contracts N^o 137–2017 "Microbiological examination of the walls with frescoes in the monument of the national significance - St. Sophia Cathedral, 11th century, for the presence of microorganisms" and N^o 122–2019 "Monitoring of the microbial development and mineral matrix destruction in the damaged areas of the walls with paintings in the southern parts of the monument of national significance - St. Sophia Cathedral, XI century" as well as constant guidance, support and helpful discussions of staff of "Sophia of Kyiv", especially General Director Nelya Kukovalska and Drs Vyacheslav Kornienko, Roman Gutsulyak, Anatoliy Ostapchuk, and Dorad Kaporikov. The authors are grateful to Mrs. Mykola Skoryk and Viacheslav Moskaliuk for invaluable technical support at Tescan Mira 3 LMU microscope, LLC Nanomedtech, Kyiv, Ukraine. Financial support of the Geomicrobiology Group (GMG) is received from the Natural Environment Research Council [NE/M01090/1(TeASe); NE/M011275/1 (CoG^3)] which is gratefully acknowledged. The comments and criticism of three anonymous reviewers helped to improve this manuscript.

Appendix A. Supplementary data

Supplementary data to this article can be found online at https://doi.org/10.1016/j.ibiod.2022.105486.

References

Addinsoft, 2021. XLSTAT Statistical and Data Analysis Solution. New York, USA. https://www.xlstat.com.

Banfield, J.P., Barker, W.W., Welch, S.A., Taunton, A., 1999. Biological impact on mineral dissolution: application of the lichen model to understanding mineral weathering in the rhizosphere. Proceedings of the National Academy of Sciences of the USA 96, 3404–3411. https://doi.org/10.1073/pnas.96.7.3404.

Barrett, G.T., Donnelly, C., Reimer, P.J., 2020. Radiocarbon dating mortar: the identification of a Medieval Irish round tower using a multi-method intercomparative approach. J. Archaeol. Sci.: Report 33, 102538. https://doi.org/10.1016/j.jasrep.2020.102538.

Bastian, F., Jurado, V., Nováková, A., Alabouvette, C., Saiz-Jimenez, C., 2010. The microbiology of Lascaux cave. Microbiology 156, 644–652. https://doi.org/10.1099/mic.0.036160-0.

Bates, S.T., Garcia-Pichel, F., 2009. A culture-independent study of freeliving fungi in biological soil crusts of the Colorado Plateau: their diversity and relative contribution to microbial biomass. Environ. Microbiol. 11, 56–67. https://doi.org/10.1111/j.1462-2920.2008.01738.x.

Burford, E.P., Fomina, M., Gadd, G.M., 2003. Fungal involvement in bioweathering and biotransformation of rocks and minerals. Mineral. Mag. 67, 1127–1155. https://doi.org/10.1180/0026461036760154.

Burgstaller, W., Schinner, F., 1993. Leaching of metals with fungi. J. Biotechnol. 27, 91–116.

Caneva, G., Isola, D., Lee, H.J., Chung, Y.J., 2020. Biological risk for hypogea: shared data from Etruscan tombs in Italy and ancient tombs of the Baekje Dynasty in Republic of Korea. Appl. Sci. 10, 6104. https://doi.org/10.3390/app10176104.

Chi, Z., Wang, Z.-P., Wang, G.-Y., Khan, I., Chi, Z.-M., 2016. Microbial biosynthesis and secretion of L-malic acid and its applications. Crit. Rev. Biotechnol. 36, 99–107. https://doi.org/10.3109/07388551.2014.924474.

Ciferri, O., 1999. Microbial degradation of paintings. Appl. Environ. Microbiol. 65, 879–885.
Coutinho, M.L., Miller, A.Z., Macedo, M.F., 2015. Biological colonization and biodeterioration of architectural ceramic materials: an overview. J. Cult. Herit. 16, 759–777. https://doi.org/10.1016/j.culher.2015.01.006.
Ehrlich, H.L., 1996. How microbes influence mineral growth and dissolution. Chem. Geol. 132, 5–9. https://doi.org/10.1016/S0009-2541(96)00035-6.
Elhagrassy, A.F., 2018. Isolation and characterization of actinomycetes from mural paintings of Snu-Sert-Ankh tomb, their antimicrobial activity, and their biodeterioration. Microbiol. Res. 216, 47–55.
Ettenauer, J., Piñar, G., Tafer, H., Sterflinger, K., 2014. Quantification of fungal abundance on cultural heritage using real time PCR targeting the β-actin gene. Front. Microbiol. 5, 262. https://doi.org/10.3389/fmicb.2014.00262.
Feng, Q., Ma, X., Zhang, X., Li, Z., Li, S., 1998. Study on microbial factor on color change of Dunhuang mural I. Classification of microbes on color-changed mural and property of some typical species. Acta Microbiol. Sin. 38, 52–56.
Fierer, N., Jackson, J.A., Vilgalys, R., Jackson, R.B., 2005. Assessment of soil microbial community structure by use of taxon-specific quantitative PCR assays. Appl. Environ. Microbiol. 71, 4117–4120. https://doi.org/10.1128/aem.71.7.4117-4120.2005.
Fogel, G., Collins, C., Li, J., Brunk, C.F., 1999. Prokaryotic genome size and SSU rDNA copy number: estimation of microbial relative abundance from a mixed population. Microb. Ecol. 38, 93–113. https://doi.org/10.1007/s002489900162.
Fomina, M., Podgorsky, V.S., Olishevska, S.V., Kadoshnikov, V.M., Pisanska, I.R., Hillier, S., Gadd, G.M., 2007. Fungal deterioration of barrier concrete used in nuclear waste disposal. Geomicrobiol. J. 24, 643–653. https://doi.org/10.1080/01490450701672240.
Gadd, G.M., 2007. Geomycology: biogeochemical transformations of rocks, minerals, metals and radionuclides by fungi, bioweathering and bioremediation. Mycol. Res. 111, 3–49. https://doi.org/10.1016/j.mycres.2006.12.001.
Gadd, G.M., 2010. Metals, minerals and microbes: geomicrobiology and bioremediation. Microbiology 156, 609–643. https://doi.org/10.1099/mic.0.037143-0.
Gadd, G.M., 2017. Geomicrobiology of the built environment. Nature Microbiology 2, 1–9. https://doi.org/10.1038/nmicrobiol.2016.275.
Gadd, G.M., Bahri-Esfahani, J., Li, Q., Rhee, Y.J., Wei, Z., Fomina, M., Liang, X., 2014. Oxalate production by fungi: significance in geomycology, biodeterioration and bioremediation. Fungal Biology Reviews 28, 36–55. https://doi.org/10.1016/j.fbr.2014.05.001.
Garg, K.L., Jain, K.K., Mishra, A.K., 1995. Role of fungi in the deterioration of wall paintings. Sci. Total Environ. 167, 255–271. https://doi.org/10.1016/0048-9697(95)04587-q.
Kalra, R., Conlan, X.A., Goel, M., 2020. Fungi as a potential source of pigments: harnessing filamentous fungi. Front. Chem. 8, 369. https://doi.org/10.3389/fchem.2020.00369.
Karpovich-Tate, N., Rebrikova, N.L., 1991. Microbial communities on damaged frescoes and building materials in the Cathedral of the Nativity of the Virgin in the Pafnutii-Borovskii monastery, Russia. Int. Biodeterior. 27, 281–296. https://doi.org/10.1016/0265-3036(91)90057-X.
Knabe, N., Gorbushina, A.A., 2018. Territories of rock-inhabiting fungi: survival on and alteration of solid air-exposed surfaces. Methods Microbiol. 45, 145–169. https://doi.org/10.1016/bs.mim.2018.06.001.
Kobayashi, T., Sasaki, M., 2017. Ribosomal DNA stability is supported by many 'buffer genes'-introduction to the Yeast rDNA Stability Database. FEMS Yeast Res. 17 https://doi.org/10.1093/femsyr/fox001. PMID: 28087673.
Kövilein, A., Kubisch, C., Cai, L., Ochsenreither, K., 2020. Malic acid production from renewables: a review. J. Chem. Technol. Biotechnol. 95, 513–526. https://doi.org/10.1002/jctb.6269.
Kumar, R., Kumar, A., 1999. Biodeterioration of Stone in Tropical Environments: an Overview. The J. Paul Getty Trust, Madison,WI, USA.
Kwan, E.X., Wang, X.S., Amemiya, H.M., Brewer, B.J., Raghuraman, M.K., 2016. rDNA copy number variants are frequent passenger mutations in *Saccharomyces cerevisiae* deletion collections and de novo transformants. G3 (Bethesda) 6, 2829–2838. https://doi.org/10.1534/g3.116.030296.
Lagashetti, A.C., Dufossé, L., Singh, S.K., Singh, P.N., 2019. Fungal pigments and their prospects in different industries. Microorganisms 7, 604. https://doi.org/10.3390/microorganisms7120604.
Liang, X., Kierans, M., Ceci, A., Hillier, S., Gadd, G.M., 2015. Phosphatase-mediated bioprecipitation of lead by soil fungi. Environ. Microbiol. 18, 219–231. https://doi.org/10.1111/1462-2920.13003.
Liu, Z., Zhang, Y., Zhang, F., Hu, C., Liu, G., Pan, J., 2018. Microbial community analyses of the deteriorated storeroom objects in the Tianjin museum using culture-independent and culture-dependent approaches. Front. Microbiol. 9, 802. https://doi.org/10.3389/fmicb.2018.00802.
Lloyd, J.R., 2003. Microbial reduction of metals and radionuclides. FEMS (Fed. Eur. Microbiol. Soc.) Microbiol. Rev. 27, 411–425. https://doi.org/10.1016/S0168-6445(03)00044-5.
Ma, W., Wu, F., Tian, T., He, D., Zhang, Q., Gu, J.-D., Duand, Y., Ma, D., Wang, W., Feng, H., 2020. Fungal diversity and its contribution to the biodeterioration of mural paintings in two 1700-year-old tombs of China. Int. Biodeterior. Biodegrad. 152, 104972 https://doi.org/10.1016/j.ibiod.2020.104972.
Massart, D.L., Vandeginste, B.G.M., Buydens, L.M.C., de Jong, S., Lewi, P.J., Smeyers Verbeke, J., 1998. Handbook of Chemometrics and Qualimetrics. Part B. Elsevier Science, Amsterdam.
Melo, D., Sequeira, S.O., Lopes, J.A., Macedo, M.F., 2019. Stains versus colourants produced by fungi colonising paper cultural heritage: a review. J. Cult. Herit. 35, 161–182.
Michaelsen, A., Piñar, G., Pinzari, F., 2010. Molecular and microscopical investigation of the microflora inhabiting a deteriorated Italian manuscript dated from the thirteenth century. Environ. Microbiol. 60, 69–80. https://doi.org/10.1007/s00248-010-9667-9.
Milanesi, C., Baldi, F., Vignani, R., Ciampolini, F., Faleri, C., Cresti, M., 2006. Fungal deterioration of medieval wall fresco determined by analysing small fragments containing copper. Int. Biodeterior. Biodegrad. 57, 7–13. https://doi.org/10.1016/j.ibiod.2005.10.002.
Money, N.P., 2004. The fungal dining habit–a biomechanical perspective. Mycologist 18, 71–76. https://doi.org/10.1017/S0269-915X(04)00203-4.
Nugari, M.P., Pietrini, A.M., Caneva, G., Imperi, F., Visca, P., 2009. Biodeterioration of mural paintings in a rocky habitat: the crypt of the Original Sin (Matera, Italy). Int. Biodeterior. Biodegrad. 63, 705–711.
Pangallo, D., Kraková, L., Chovanová, K., Šimonovičová, A., De Leo, F., Urzì, C., 2012. Analysis and comparison of the microflora isolated from fresco surface and from surrounding air environment through molecular and biodegradative assays. World J. Microbiol. Biotechnol. 28, 2015–2027. https://doi.org/10.1007/s11274-012-1004-7.
Pepe, O., Sannino, L., Palomba, S., Anastasio, M., Blaiotta, G., Villani, F., Moschetti, G., 2010. Heterotrophic microorganisms in deteriorated medieval wall paintings in southern Italian churches. Microbiol. Res. 165, 21–32. https://doi.org/10.1016/j.micres.2008.03.005.
Pinna, D., 2021. Microbial growth and its effects on inorganic heritage materials. In: Joseph, E. (Ed.), Microorganisms in the Deterioration and Preservation of Cultural Heritage. Springer, Cham. https://doi.org/10.1007/978-3-030-69411-1_1.
Pinzari, F., Cornish, L., Jungblut, A.D., 2019. Skeleton bones in museum indoor environments offer niches for fungi and are affected by weathering and deposition of secondary minerals. Environ. Microbiol. 22, 59–75. https://doi.org/10.1111/1462-2920.14818.
Piñar, G., Sterflinger, K., 2021. Natural sciences at the service of art and cultural heritage: an interdisciplinary area in development and important challenges. Microb. Biotechnol. 14 https://doi.org/10.1111/1751-7915.13766.
Piñar, G., Sclocchi, M.C., Pinzari, F., Colaizzi, P., Graf, A., Sebastiani, M.L., Sterflinger, K., 2020. The microbiome of Leonardo da Vinci's drawings: a bio-archive of their history. Front. Microbiol. 11, 593401 https://doi.org/10.3389/fmicb.2020.593401.
Salim, D., Bradford, W.D., Freeland, A., Cady, G., Wang, J., Pruitt, S.C., Gerton, J.L., 2017. DNA replication stress restricts ribosomal DNA copy number. PLoS Genet. 13, e1007006 https://doi.org/10.1371/journal.pgen.1007006.
Salvadó, N., Butí, S., Pradell, T., Beltran, V., Cinque, G., Juanhuix, J., Font, L., Senserrich, R., 2016. Low molecular weight organic acid salts, markers of old fungi activity in wall paintings. Anal. Methods 8, 1637–1645. https://doi.org/10.1039/c5ay02656c.
Sand, W., Bock, E., 1991a. Biodeterioration of mineral materials by microorganisms: biogenic sulphuric and nitric-acid corrosion of concrete and natural stone. Geomicrobiol. J. 9, 129–138. https://doi.org/10.1080/01490459109385994.
Sand, W., Bock, E., 1991b. Biodeterioration of ceramic materials by biogenic acids. Int. Biodeterior. 27, 175–183.
Sklenář, F., Jurjević, Ž., Zalar, P., Frisvad, J.C., Visagie, C.M., Kolařík, M., Houbraken, J., Chen, A.J., Yilmaz, N., Seifert, K.A., Coton, M., Déniel, F., Gunde-Cimerman, N., Samson, R.A., Peterson, S.W., Hubka, V., 2017. Phylogeny of xerophilic aspergilli (subgenus *Aspergillus*) and taxonomic revision of section Restricti. Stud. Mycol. 88, 161–236. https://doi.org/10.1016/j.simyco.2017.09.002.
Sterflinger, K., 2000. Fungi as geologic agents. Geomicrobiological Journal 17, 97–124. https://doi.org/10.1080/01490450050023791.
Sugiyama, J., Kiyuna, T., Nishijima, M., An, K.-D., Nagatsuka, Y., Tazato, N., Handa, Y., Hata-Tomita, J., Sato, Y., Kigawa, R., Sano, C., 2017. Polyphasic insights into the microbiomes of the takamatsuzuka tumulus and kitora tumulus. J. Gen. Appl. Microbiol. 63, 63–113. https://doi.org/10.2323/jgam.2017.01.007.
Tazaki, K., 2013. Clays, microorganisms and biomineralization. In: Bergaya, F., Lagaly, G. (Eds.), Developments in Clay Science, vol. 5. Elsevier, Amsterdam, pp. 613–653. https://doi.org/10.1016/B978-0-08-098258-8.00019-5.
Tomassetti, M.C., Cirigliano, A., Arrighi, C., Negri, R., Mura, F., Maneschi, M.L., Gentili, M.D., Stirpe, M., Mazzoni, C., Rinaldi, T., 2017. A role for microbial selection in frescoes' deterioration in *Tomba degli Scudi* in Tarquinia, Italy. Sci. Rep. 7 (6027), 1–8. https://doi.org/10.1038/s41598-017-06169-0.
Turnau, K., Jędrzejczyk, R.J., Ważnyb, R., Chlebda, D., Janicka, M., Pawcenis, D., Łojewski, T., 2020. Microbes of XVI century arrases of krakow royal castle. Microbiol. Res. 238, 126485 https://doi.org/10.1016/j.micres.2020.126485.
Unković, N., Dimkić, I., Stupar, M., Stanković, S., Vukojević, J., Ljaljević Grbić, M., 2018. Biodegradative potential of fungal isolates from sacral ambient: in vitro study as risk assessment implication for the conservation of wall paintings. PLoS One 13, e0190922. https://doi.org/10.1371/journal.pone.0190922.
Vasanthakumar, A., DeAraujo, A., Mazurek, J., Schilling, M., Mitchell, R., 2013. Microbiological survey for analysis of the brown spots on the walls of the tomb of King Tutankhamun. Int. Biodeterior. Biodegrad. 79, 56–63. https://doi.org/10.1016/j.ibiod.2013.01.014.
Visagie, C.M., Yilmaz, N., Renaud, J.B., Sumarah, M.W., Hubka, V., Frisvad, J.C., Chen, A.J., Meijer, M., Seifert, K.A., 2017. A survey of xerophilic *Aspergillus* from indoor environment, including descriptions of two new section *Aspergillus* species producing eurotium-like sexual states. MycoKeys 19, 1–30. https://doi.org/10.3897/mycokeys.19.11161.
Vrabl, P., Fuchs, V., Pichler, B., Schinagl, C.W., Burgstaller, W., 2012. Organic acid excretion in *Penicillium ochrochloron* increases with ambient pH. Front. Microbiol. 3, 121. https://doi.org/10.3389/fmicb.2012.00121.